Field-portable x-ray fluorescence spectrometer use in volcanogenic massive sulphide exploration with examples from the Touleary occurrence (MINFILE Occurrence 115O 176) in west-central Yukon

Patrick J. Sack[1], Lara L. Lewis
Yukon Geological Survey, Whitehorse, YT

Sack, P.J. and Lewis, L., 2013. Field-portable x-ray fluorescence spectrometer use in volcanogenic massive sulphide exploration with examples from the Touleary occurence (MINFILE Occurrence 115O 176) in west-central Yukon. *In:* Yukon Exploration and Geology 2012, K.E. MacFarlane, M.G. Nordling, and P.J. Sack (eds.), Yukon Geological Survey, p. 115-131.

ABSTRACT

Field-portable x-ray fluorescence analysers (pXRF) are becoming a common tool in the savvy mineral explorer's tool kit. Benefits include portability and ease of use, real-time acquisition of XRF data with minimal processing, immediate availability and analysis of data in the field, and a reasonably large number of elements that can be measured reliably. The findings indicate that data for 15 elements obtained with an Innov-X Omega pXRF analyser (2010 version) correlate well with lithogeochemical whole-rock analyses with R^2 values generally ≥0.7. The difference in elemental abundances between pXRF analyses of thin section off-cuts (a proxy for drill core) and pulps from the whole-rock analyses are generally ±35%, indicating that no sample preparation is needed for the rock samples analysed in this study. The uncorrected pXRF values of some elements can be very similar to whole-rock analytical abundances; however, it is recommended that uncorrected pXRF data only be used semi-quantitatively, such as for downhole elemental plots in which relative patterns or trends are more informative than individual data points. For more sophisticated plots such as those combining elements into ratios to form alteration indices, corrected pXRF data should be used. The pXRF data are also adequate for construction of simple volcanic composition plots that can be used to aid in identification of protolith compositions of altered samples. The pXRF is well suited to volcanogenic massive sulphide exploration as the analytical data obtained from drill core (using thin section off-cuts as a proxy) are comparable to whole-rock analyses and the range of immobile and mobile, major and trace elements should be versatile enough for most exploration programs. However, pXRF shouldn't be viewed as a replacement to traditional whole-rock geochemical methods.

[1]*patrick.sack@gov.yk.ca*

INTRODUCTION

Field-portable x-ray fluorescence analyzers (pXRF) are proving to be a valuable tool for exploration as they are portable, simple to use, can simultaneously analyse over 20 elements, and depending on conditions, can produce meaningful results (Peter *et al.*, 2009). As part of a larger project investigating the recently discovered Touleary volcanogenic massive sulphide (VMS) occurrence (MINFILE Occurrence 115O 176), 15 samples of diamond drill core were analysed using both traditional laboratory whole-rock lithogeochemical and pXRF analytical methods; both thin section off-cuts (a proxy for cut diamond drill core) and the pulps from the whole-rock geochemical samples were analysed with the pXRF. The goal of the pXRF study was to evaluate the precision and accuracy of such analyses against those of traditional whole-rock methods, determine if sample preparation (off-cuts vs. pulps) is important, and evaluate the usefulness of the pXRF for VMS exploration.

GEOLOGY

The Touleary occurrence (63°0′24.48″N, 139°8′11.85″W) is located within Yukon-Tanana terrane rocks, approximately 125 km south of Dawson City (Fig. 1). The occurrence is located between the north and south forks of Kirkman Creek in a fault-bound block of southeast dipping amphibolite schist/gneiss metabasites interlayered with minor metafelsite (Ryan and Gordey, 2001a,b).

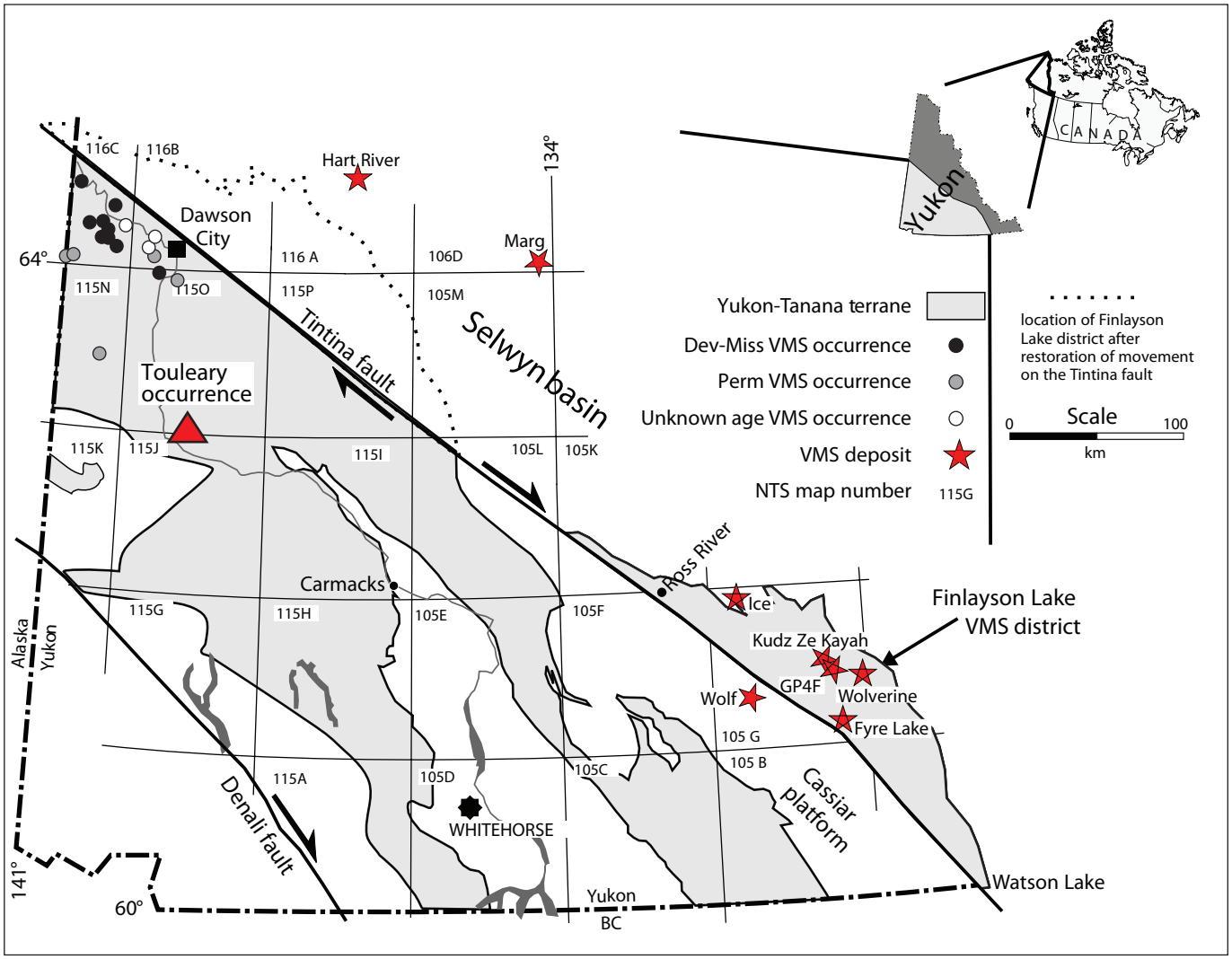

Figure 1. *Location of significant VMS deposits in Yukon and VMS occurrences in the Dawson City area (modified from Hunt, 2002). Also shown are the locations of the Yukon-Tanana terrane (YTT), the Finlayson Lake VMS district, and the approximate location of the Finlayson Lake VMS district after restoration of movement along the Tintina fault. Dev-Miss = Late Devonian to mid-Mississippian VMS occurrences, Perm = Permian VMS occurrences; based on Hunt (2002).*

Intense regional deformation and garnet amphibolite-facies metamorphism have hindered identification of the protolith of these rocks; however, they are interpreted to be of volcanic and volcaniclastic origin. The interfingering of metabasite and metafelsite suggests a bimodal nature, possibly in an arc setting (Ryan and Gordey, 2001a,b). These rocks are thought to be Devonian to Mississippian in age (Gordey and Ryan, 2005) and may correlate with rocks of a similar age in the Finlayson Lake VMS district (Fig. 1). However, several plutonic and hypabyssal rocks in the vicinity of the study area have yielded only Permian ages; therefore, it is also possible that these metavolcanic rocks are correlative locally with the Permian Klondike Schist in the Dawson Range near the Boulevard mineral occurrence, 24 km southwest of Touleary (J. Ryan, pers. comm., 2012).

SUMMARY OF DIAMOND DRILL CORE LOGGING

Diamond drilling in 2011 by Arcus Development Group Inc. targeted a linear magnetic low anomaly that is coincident with the contact between mafic schist (Unit 8) and amphibolite (Unit 6) on the map of Ryan and Gordey (2001a) (H. Burrell, pers. comm., 2012). This drilling intersected stratiform, semi-massive to massive sulphide mineralization dominated by pyrite and chalcopyrite. The 15 samples used in this study are from diamond drill hole TL11-05 that cored two semi-massive to massive sulphide intersections. The upper intersection is 2.25 m, grading 7.2% Cu, 116 g/t Ag, 3.6 g/t Au, and 4.3% Zn; the lower is 14.15 m thick and grades 1.4% Cu, 17 g/t Ag, 0.8 g/t Au, and 0.3% Zn (Arcus news release, October 4, 2011). Hydrothermal alteration is characterized by an intense quartz + pyrite ± sericite assemblage below mineralization that gradually transitions to chlorite ± sericite above and below mineralization. The nature of mineralization, alteration, and the host volcanic rocks are consistent with Touleary having a volcanogenic massive sulphide genetic origin.

Diamond drill hole TL11-05 is 246.28 m long with bedrock intersected at 3.0 m. The rocks are fine to coarse-grained schist with a grain size typically ranging from 0.5 mm to 5 mm; a few crystals can be larger than 1 cm. Layering, where present, is thin to thick (1 cm to 50 cm) and likely represents both primary features (bedding) and metamorphic features. Figure 2 shows a graphic lithologic log with accompanying photos and a log of the dominant hydrothermal alteration minerals. The rocks are commonly pale to dark green and are dominated by chlorite ± muscovite; garnet porphyroblasts up to 1 cm are common in places. The rock textures are heavily modified by hydrothermal alteration and subsequent regional metamorphism and deformation. Most primary textures have been destroyed; however, these rocks are interpreted to have a volcanic and volcaniclastic origin. Based on rock textures and mineralogy the succession is divided into two series: 1) an upper massive to weakly stratified, pale green felsic volcanic series and 2) a lower, thinly to thickly layered dark green mafic volcanic series (Fig. 6).

ANALYTICAL METHODS

WHOLE-ROCK METHODS

Diamond drill core samples were split and only fresh rock free of oxidized surfaces were submitted for analysis. Whole-rock analyses were conducted at Activation Laboratories Ltd., Ancaster, Ontario, using their 4Lithoresearch analytical package, a lithium metaborate/tetraborate fusion followed by analysis using Inductively Coupled Plasma Mass Spectrometry (ICPMS). For major elements, the quality of these data meets or exceeds fusion x-ray fluorescence data. For trace elements, the fusion process provides total dissolution of refractory minerals such as zircon, sphene, and monazite, and gives accurate rare earth and high field strength element data. Using this analytical package, detection limits for major elements are 0.001% to 0.01% and trace elements are typically better than 1 ppm. However, in order to lower detection limits for As, Au, Br, Cr, Ir, Sc, and Se, these elements were analysed by Instrumental Neutron Activation Analysis (INAA), and for Cd, Cu, Ni, S, and Zn, a multi-acid digestion followed by ICPMS analysis was used. A complete list of elements, analytical method and respective detection limits is reported in Table 1.

PXRF METHODS

The hand-held pXRF analyzer used in this study is an Innov-X Omega analyser manufactured by Innov-X-Systems Inc. (now Olympus Corporation) that was purchased in 2010. This instrument is equipped with a silver anode x-ray tube that operates at 40 kV and a maximum of 4 watts with a silicon positive-intrinsic negative (SiPIN) detector. The SiPIN detector technology has now been surpassed by silicon drift detectors (SDD) that have better detection limits; however, pXRF with SiPIN detectors are still common and are less expensive than SDD models.

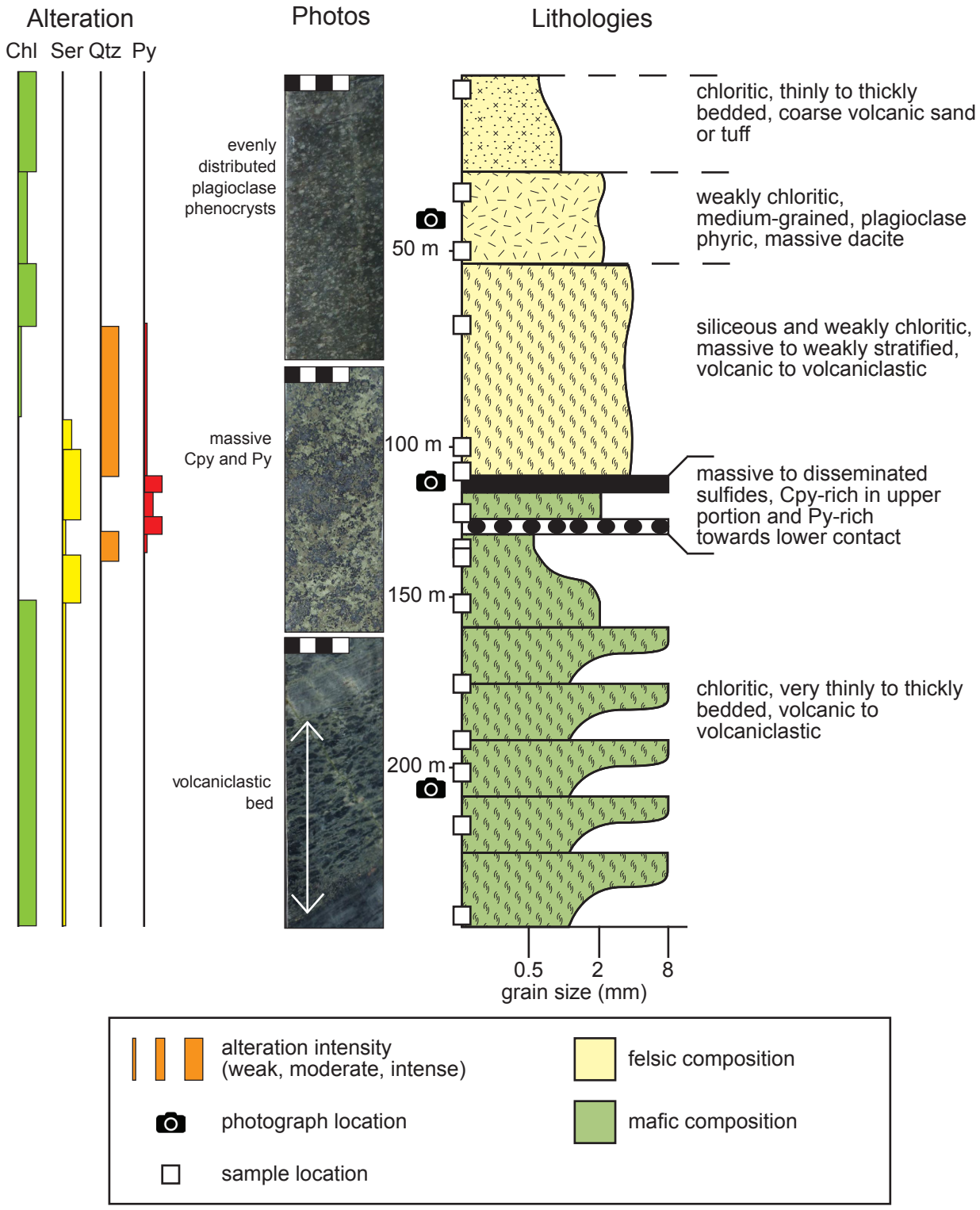

Figure 2. *Graphic log of TL11-05 with representative photos and a log of visual alteration mineralogy and intensity. Scale bars in photos are cm divisions. Chl = chlorite, Ser = sericite, Qtz = quartz, Py = pyrite, and Cpy = chalcopyrite. Composition based on Ti /Zr vs. Nb/Y (Winchester and Floyd, 1977) using whole-rock data.*

Table 1. *Detection limits (in ppm except major oxides) for elements analysed by Activation Laboratories Ltd. using whole-rock methods described in text. White = fusion digestion, light grey = INAA, and dark grey = multi-acid digestion.*

Element	Detection Limit	Element	Detection Limit
Al2O3	0.01%	Rb	1
CaO	0.01%	S	100
Fe2O3	0.01%	Sb	0.2
K2O	0.01%	Sc	0.1
MgO	0.01%	Se	3
MnO	0.001%	Sn	1
Na2O	0.01%	Sr	2
P2O5	0.01%	Ta	0.01
SiO2	0.01%	Th	0.05
TiO2	0.001%	Tl	0.05
Ag	0.5	U	0.01
As	0.5	V	5
Au	0.002	W	0.5
Ba	3	Y	0.5
Be	1	Zn	1
Bi	0.1	Zr	1
Br	0.5	La	0.05
Cd	0.5	Ce	0.05
Co	1	Pr	0.01
Cr	5	Nd	0.05
Cs	0.1	Sm	0.01
Cu	10	Eu	0.005
Ga	1	Gd	0.01
Ge	0.5	Tb	0.01
Hf	0.1	Dy	0.01
In	0.1	Ho	0.01
Ir	0.005	Er	0.01
Mo	2	Tm	0.005
Nb	0.2	Yb	0.01
Ni	1	Lu	0.002
Pb	5		

The pXRF is capable of measuring elements with atomic numbers between 15 (phosphorus) and 82 (lead), excluding the lanthanide elements and noble gases (Fig. 3). The pXRF analyses were conducted in 'soil mode', which is a two-beam mode employing an internal Compton Normalization calibration. This mode is optimized for sample types with a predominantly light element matrix (*e.g.*, soils, tills, and rocks) and has detection levels between 5 and 200 ppm with the exception of P and Al which are 0.5% and 1.0% respectively (Innov-X-Systems, 2009). Each analysis was two minutes in total with one minute using beam 1 conditions (heavy option: Ti and heavier elements) and one minute using beam 2 (light and transition elements: Fe and lighter elements).

Samples in this study were collected in the field and analysed with the pXRF in Whitehorse. Thin section off-cuts (minimum 5 mm thick) were dried and analysed such that the analyser window was oriented perpendicular to foliation, giving a cross sectional analysis not confined to a single foliation surface. The analysing window was positioned on a visually representative, fine-grained portion of the off-cut, avoiding unrepresentative features such as porphyroblasts. Pulps from the laboratory geochemical samples and a diorite gneiss Canadian Certified Reference Material pulp (SY-4) were compacted to form a compressed sample at least 5 mm thick as recommended by the manufacturer (Innov-X-Systems, 2009); three different spots were analysed through the plastic sample bag and the results were averaged for each element; no correction was made for potential contamination from the sample bags.

To evaluate the reliability of the data for each element, the pXRF off-cut and pulp data were plotted against the laboratory whole-rock data and the slope of a best fit line through the data and its corresponding coefficient of determination (R^2) and y-intercept value were calculated. Elements with a strong coefficient of determination ($R^2 \geq 0.7$) are deemed reliable and are corrected using the slope and intercept of the line of best fit to the pulp data (Table 2).

RESULTS

Geochemical studies of VMS deposits tend to utilize elements useful for determining primary geochemical features (immobile elements) or alteration geochemical features (mobile elements) (*e.g.*, Barrett *et al.*, 1993; Chapman *et al.*, 2009; Large *et al.*, 2001; MacLean and Barrett, 1993; Mireku and Stanley, 2006). In consideration of both element mobility (Pearce, 1996) and the element range possible with the pXRF used, the focus was on the following immobile elements: Ti, V, Cr, Y, Zr, and Nb; elements with variable behaviour (mobile to immobile): P, Mn, Fe, Ni, As, Sn, and Sb; and mobile elements: K, Ca, Cu, Zn, Rb, Sr, Ba, Au, and Pb (Fig. 3). In the discussion, variable and mobile elements are grouped into a single category. For both immobile and mobile elements, R^2 of

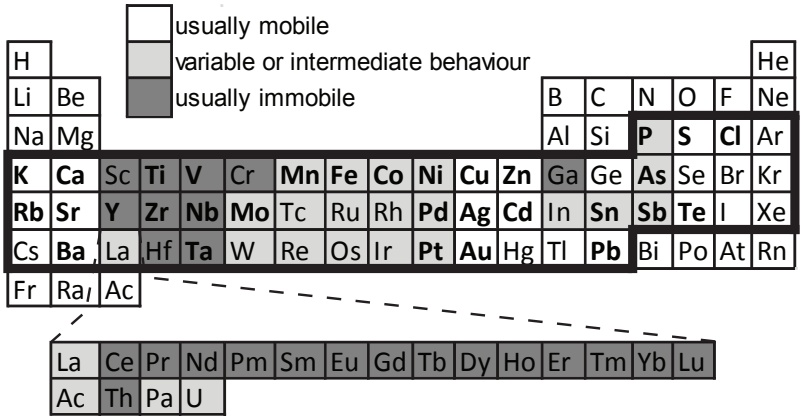

Figure 3. *Periodic table with elements coded according to mobility during alteration (modified from Pearce, 1996). Outline shows the range of elements that can be analysed with the pXRF analyser used in this study. Elements in bold are those included in the 'soil mode'.*

the pulp data is generally slightly higher than that for the thin section off-cut data; ascribed as a subtle nugget effect in the off-cuts that is nullified in the pulps when they are pulverized and homogenized. However, the difference between pXRF analytical data for thin section off-cuts (a proxy for drill core) and pulps from the whole-rock analyses is generally ≤35%, indicating that no sample preparation is needed for the rock samples analysed in this study. Whole-rock and pXRF (raw and corrected) data are included, respectively, in Appendices 1 and 2.

IMMOBILE ELEMENTS

The immobile elements Ti, V, Cr, Y, Zr, and Nb are part of the pXRF analytical package used (Fig. 3). Figure 4 a-e shows the correlation between the laboratory whole-rock and pXRF analyses of both pulps and thin section off-cuts, and Table 2 summarizes elemental variations for all three sets of analyses. For both pulps and off-cuts, Ti, Zr, Y, and Cr have $R^2 \geq 0.7$, suggesting good correlation between the data for the two pXRF sample types and between pXRF and whole-rock data. Vanadium has R^2 of 0.07 and 0.05 for pulps and off-cuts, respectively, as a result of interference with Ba when laboratory whole-rock Ba values are >2000 ppm. Nb values determined by laboratory whole-rock analysis range between 1 and 17 ppm, and this is below the pXRF lower limit of detection (20 ppm) which is too high to be of use in this study. Of the six immobile elements investigated in this study, only Ti and Zr are routinely above detection in pXRF analyses of thin section off-cuts with good determination coefficients (Table 2).

MOBILE ELEMENTS

Figure 5 a-f shows the correlation between selected whole-rock and pXRF analyses of both pulps and thin section off-cuts. Data from precious metals Au and Ag are not usable as the pXRF detection limit for Au is 10 ppm, much too high to be of use in this study, and the Ag anode in the analyser used causes over estimation of Ag. Nickel, chlorine, and niobium can be analysed on the pXRF used in this study, but their abundances in the samples studied are below the lower limits of detection (*e.g.*, Ni ranges from 2 to 39 ppm in whole-rock analyses, but was not detected in off-cuts). Cadmium, phosphorus, tin, and tantalum all have $R^2<0.5$ and slopes ranging from -0.01 to +7.36 demonstrating that these elements are poorly correlated and cannot be corrected using a linear correction. The following elements are found to have good determination coefficients (mostly ≥0.7): As, Ba, Ca, Co, Cu, Fe, K, Mn, Pb, Rb, S, and Sr (Table 2).

DISCUSSION

The primary aim of this study was to evaluate the utility of determining gross lithogeochemical characteristics in the field, such as mobile element variation due to hydrothermal alteration. For this purpose, a simple approach to the treatment of the pXRF data has been devised: 1) a focus on elements with high determination coefficients ($R^2 \geq 0.7$) that can be corrected using a simple linear equation of a best fit line; 2) major element data in this paper are elemental rather than in oxide form as is the norm in whole-rock data sets; and 3) focusing only on simple geochemical features that should be robust enough for preliminary interpretations. More sensitive uses, such as tectonic discrimination diagrams and alkalinity diagrams, are better suited to high-quality laboratory whole-rock data.

IMMOBILE ELEMENTS AND IGNEOUS COMPOSITION

Volcanogenic massive sulphide deposits commonly have spatially and temporally associated zones of hydrothermally altered host rocks that have obscured primary protolith textures and compositions (Gifkins *et al.*, 2005; Ishikawa *et al.*, 1976; Newberry *et al.*, 1989). Thus, a common application of whole-rock lithogeochemical data is the identification of precursor volcanic rock type

Table 2. *Summary of elemental data collected with ICP and pXRF. Elements shaded grey are determined to be reliable and are the focus of discussion. All elements are in ppm except Au which is in ppb. N = number of samples above detection limit. BD = below lower limit of detection. NA = no analysis. R^2, slope, and intercept values are calculated using the equation of a line of best fit through the whole-rock data versus the pulp or thin section off-cut data.*

Elements	Whole-rock ICP		pXRF (pulps)					pXRF (thin section off-cut)				
	Range	N	Range	N	R^2	slope	intercept	Range	N	R^2	slope	intercept
Ag	BD - 1.7	1	104 - 240	15	NA	NA	NA	114 - 283	15	NA	NA	NA
As	BD - 16.5	9	BD - 60	11	0.63	0.31	1.70	BD - 17	11	0.59	1.03	0.24
Au	BD - 412	4	1000 - 19000	15	0.29	NA	NA	BD - 14000	14	0.16	NA	NA
Ba	52 - 4702	15	237 - 2939	15	0.81	1.45	128	220 - 3238	15	0.87	1.58	51
Ca	357 - 59606	15	BD - 58013	14	0.97	1.11	3168	BD - 95467	13	0.83	0.61	7241
Cd	BD - 0.9	5	BD - 30	13	0.46	0.01	0.25	4 - 63	15	0.19	-0.01	0.57
Cl	NA	0	BD	0	NA	NA	NA	BD	0	NA	NA	NA
Co	1 - 31	15	107 - 1332	15	0.75	0.02	-2.90	151 - 1077	15	0.59	0.02	-0.61
Cr	BD - 252	6	7 - 207	15	0.93	1.32	-40	BD - 192	14	0.94	1.38	-28
Cu	2 - 7430	15	BD - 7895	5	1.00	0.94	-5	BD - 7184	4	1.00	1.03	21
Fe	31614 - 166324	15	13013 - 73121	15	0.96	2.11	13287	9060 - 91830	15	0.67	1.42	46148
K	2075 - 25818	15	1490 - 22932	15	0.96	1.06	1931	3486 - 24177	15	0.90	0.90	1176
Mn	50 - 1321	15	79 - 1418	15	0.98	1.00	-22	20 - 1865	15	0.68	0.74	224
Mo	BD - 14	3	2 - 5	15	0.57	0.38	1.17	BD - 24	6	0.50	0.33	1.57
Nb	1 - 17	15	BD	0	NA	NA	NA	BD	0	NA	NA	NA
Ni	2 - 39	15	BD	0	NA	NA	NA	BD	0	NA	NA	NA
P	87 - 698	15	BD - 15577	8	0.06	-0.01	456	517 - 33025	15	0.04	0.01	362
Pb	BD - 230	14	11 - 356	15	0.93	0.68	-0.86	8 - 313	15	0.83	0.83	3.34
Pd	NA	0	BD - 394	13	NA	NA	NA	BD - 77	9	NA	NA	NA
Pt	NA	0	BD - 37	5	NA	NA	NA	BD - 17	6	NA	NA	NA
Rb	2 - 61	15	6 - 72	15	0.88	0.67	8.53	1 - 94	15	0.81	0.81	5.47
S	150 - 73700	15	BD - 32340	8	0.95	2.41	2444	BD - 64612	8	0.96	1.11	1757
Sb	BD - 19.5	6	BD - 20	4	0.04	0.18	1.60	BD - 4	3	NA	NA	NA
Sn	BD - 4	10	BD - 48	14	0.00	7.36	1.63	BD - 31	9	0.32	0.06	1.14
Sr	26 - 499	15	27 - 481	15	0.92	1.01	-7	22 - 502	15	0.94	0.88	23
Ta	BD - 1	14	5 - 13	15	0.37	0.01	0.07	2 - 63	15	0.23	0.01	0.17
Te	NA	0	BD - 44	5	NA	NA	NA	BD 32	4	NA	NA	NA
Ti	1280 - 6685	15	1422 - 5508	15	0.88	1.11	72	1809 - 5703	15	0.68	0.91	672
V	12 - 371	15	45 - 343	15	0.07	0.29	57	34 - 523	15	0.05	0.16	75
Y	10 - 64	15	BD - 365	8	0.66	0.17	0	BD - 337	7	0.71	0.09	32
Zn	33 - 245	15	27 - 545	15	0.78	0.42	55	22 - 169	15	0.18	0.68	61
Zr	51 - 296	15	62 - 572	15	0.87	0.83	2	60 - 362	15	0.80	0.49	75

(*e.g.*, Barrett *et al.*, 1993; MacLean and Barrett, 1993). The pXRF immobile element data can be used to classify volcanic compositions, however, trace element discriminant diagrams require laboratory quality data and a diverse array of elements such as Ti, Zr, Ta, Th, Nb, Yb, and Y (*e.g.*, Barrett and MacLean, 1999; Ross and Bedard, 2009). In the pXRF element suite, Ti and Zr are the most suitable, having reasonable determination coefficients and both are present in abundances above the lower limits of detection in all samples.

To aid in the field identification of volcanic compositions, the Zr/Ti boundary between the rhyolite+dacite and andesite+basaltic andesite fields were converted on the Zr/Ti *vs.* Nb/Y diagram, revised from Winchester and Floyd (1977) in Pearce (1996), into Ti *vs.* Zr space (Fig. 6). With the exception of one highly altered sample proximal to massive sulphide, this modified diagram adequately separates the lower mafic and upper felsic rocks and there are no major differences between pXRF data obtained from off-cuts and whole-rock data (Fig. 6).

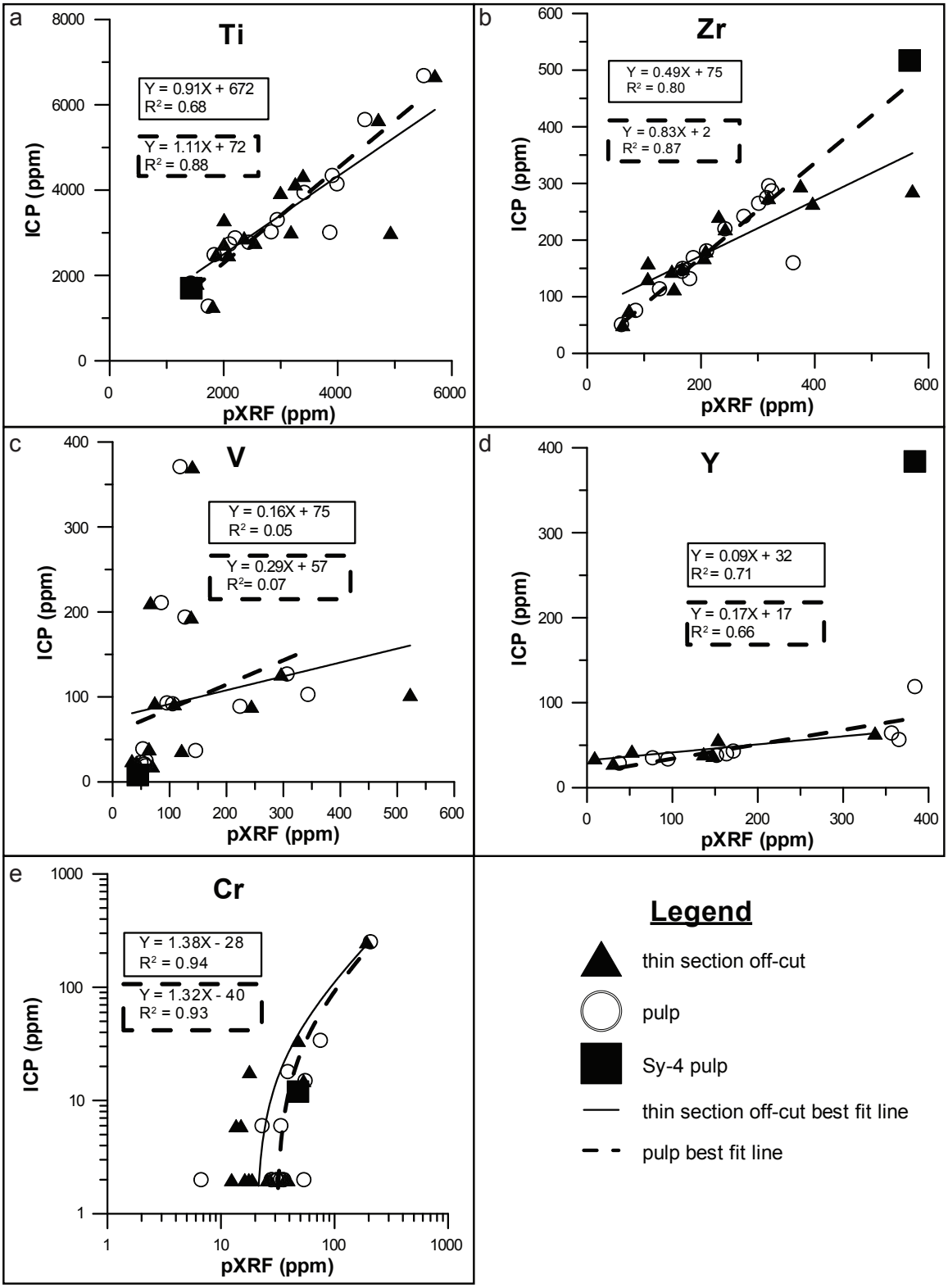

Figure 4. *Immobile element correlation plots of pXRF data (pulps and thin section off-cuts) versus laboratory ICP whole-rock data. Square symbol is a sample of Canadian Certified Reference Material SY-4, a diorite gneiss pulp.*

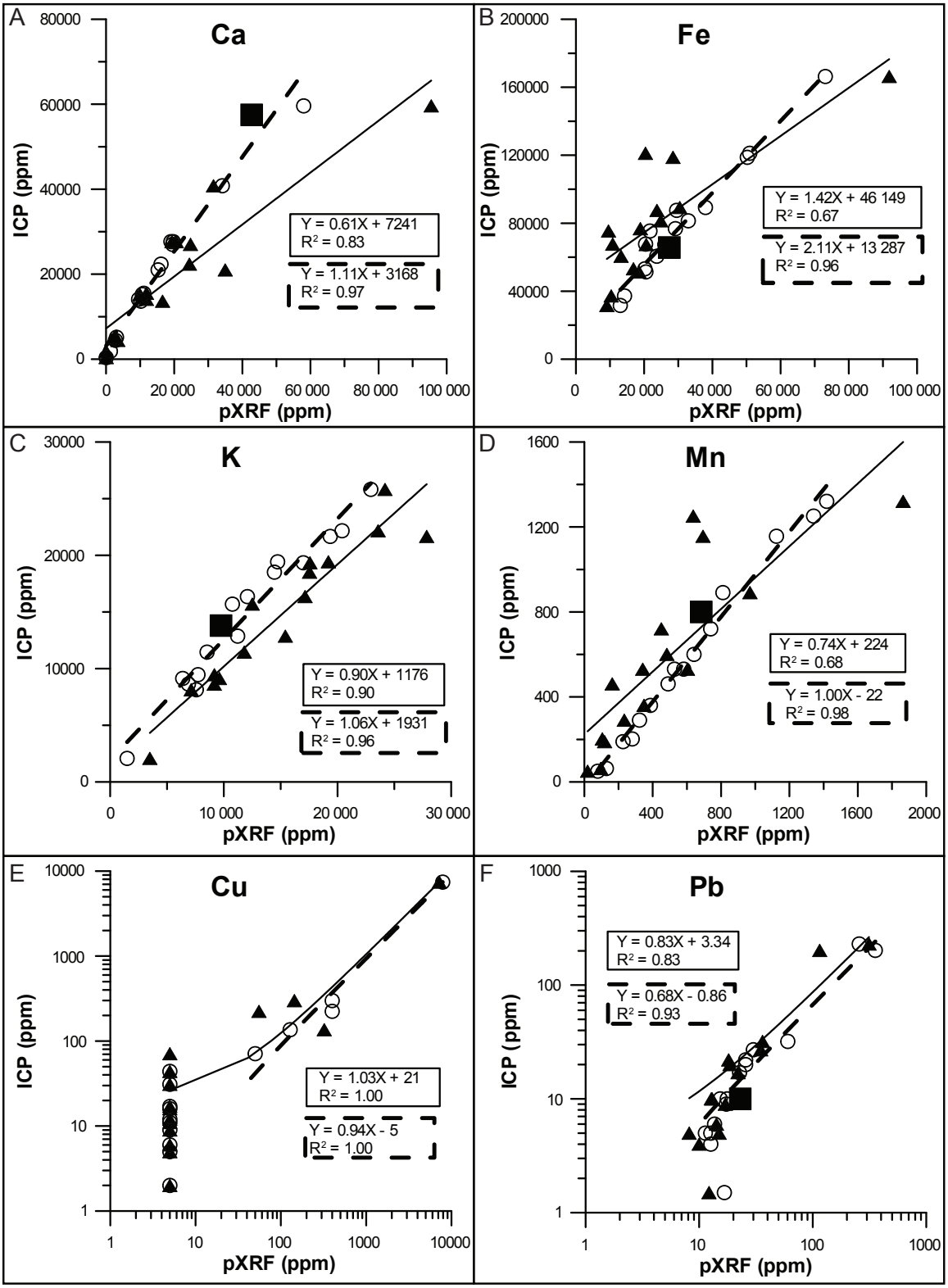

Figure 5. *Selected mobile element correlation plots of pXRF data (pulps and thin section off-cuts) versus laboratory whole-rock data. Square symbol is a sample of Canadian Certified Reference Material SY-4, a diorite gneiss pulp. Legend same as Figure 4.*

Based on this, it can be concluded that the diagram can be used as a composition discriminant to reliably separate felsic and mafic compositions. Finer subdivisions, such as intermediate compositions, require a more complete element suite and data with lower limits of detection.

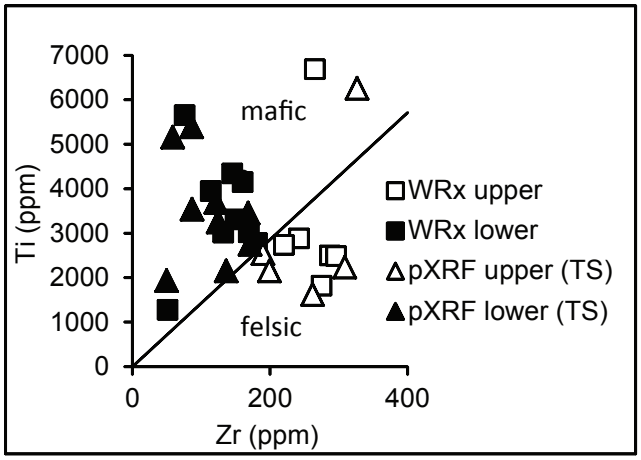

Figure 6. *Ti vs. Zr plot revised from Winchester and Floyd (1977) in Pearce (1996) using whole-rock (squares) and corrected pXRF (triangles) data from thin section off-cuts of diamond drill hole TL11-05.*

MOBILE ELEMENTS AND ALTERATION

The real-time acquisition of pXRF geochemical data in the field allows for optimization of strategies and plans. To demonstrate the usefulness of the pXRF in quantifying and mapping alteration geochemical signatures, elements that are mobile during hydrothermal alteration and traditionally employed by explorationists are evaluated using laboratory whole-rock analyses. Simple downhole plots of elements can commonly show geochemical trends relating to alteration that vary with proximity to mineralization (Gifkins *et al.*, 2005; Peter *et al.*, 2009). The data show that As, Ba, Ca, Co, Cu, Fe, K, Mn, Pb, Rb, S, and Sr mostly have good coefficients of determination ($R^2 \geq 0.7$) between both pXRF and laboratory whole-rock data. These elements are not universally present in abundances above their lower limits of detection, but because their distributions are an indicator of hydrothermal alteration intensity, abundances below the lower limits of detection are informative. The downhole patterns of both uncorrected pXRF and laboratory whole-rock data are similar for all 11 of the mobile elements mentioned above; however, the absolute values can be up to an order of magnitude different. Thus, for pXRF users who wish to use uncorrected analytical data obtained directly from the instrument, using the pXRF semi-quantitatively is recommended, such that abundance variation patterns for adjacent samples are more important than individual data values. Figure 7 shows selected downhole plots illustrating the changes in the alteration index (AI; Ishikawa *et al.*, 1976), Ca, Mn, and Pb against lithology and visually determined predominant hydrothermal alteration mineralogy. These plots reflect both lithology and alteration with the AI, Ca, and Pb plots, clearly showing geochemical anomalies proximal to mineralization.

To define alteration trends and visualize them, the alteration box plot of Large *et al.* (2001) was modified using elements deemed to be reliably determined with the pXRF. The alteration box plot of Large *et al.* (2001) plots the chlorite-carbonate-pyrite index (CCPI; see below) versus the alteration index (AI; see below) of Ishikawa *et al.* (1976). The CCPI measures the destruction and replacement of albite, K-feldspar, and sericite with Mg-Fe chlorite, whereas the AI measures the breakdown and replacement of sodic plagioclase and volcanic glass by sericite and chlorite (Large *et al.*, 2001).

The CCPI of Large *et al.* (2001) is defined as:

$$CCPI = 100(FeO+MnO)/(FeO+MnO+Na_2O+K_2O)$$

The AI of Ishikawa *et al.* (1976) is defined as:

$$AI = 100(MgO+K_2O)/(MgO+K_2O+CaO+Na_2O)$$

Because Na_2O and MgO cannot be analysed with the pXRF used, the AI formula was adapted by removing these elements. Removal of Na means the index under estimates albitic alteration (a diagenetic trend) and removal of Mg likely results in an under estimation of chlorite alteration (a hydrothermal trend) (Large *et al.*, 2001). This modified formula tends to slightly overestimate the AI value of a sample (Fig. 8). In the modified CCPI formula, Ca is assumed to have a similar behaviour to Na. The formulas modified for utilization of the pXRF data are:

$$AI = 100(K)/(K+Ca)$$

$$CCPI = 100(Fe+Mn)/(Fe+Mn+Ca+K)$$

Figure 8a shows values calculated with laboratory whole-rock data using both the original formulas (diamonds) and the modified formulas (squares). The modified values show similar patterns to the originals with the exception of several analyses from the upper part of the hole, which plot further to the lower left in the direction of diagenetic alteration (see Large *et al.*, 2001 for complete explanation of trends). Patterns to the upper right are similar, and these are the directions of hydrothermal alteration trends. Though the modified formulas slightly over estimate

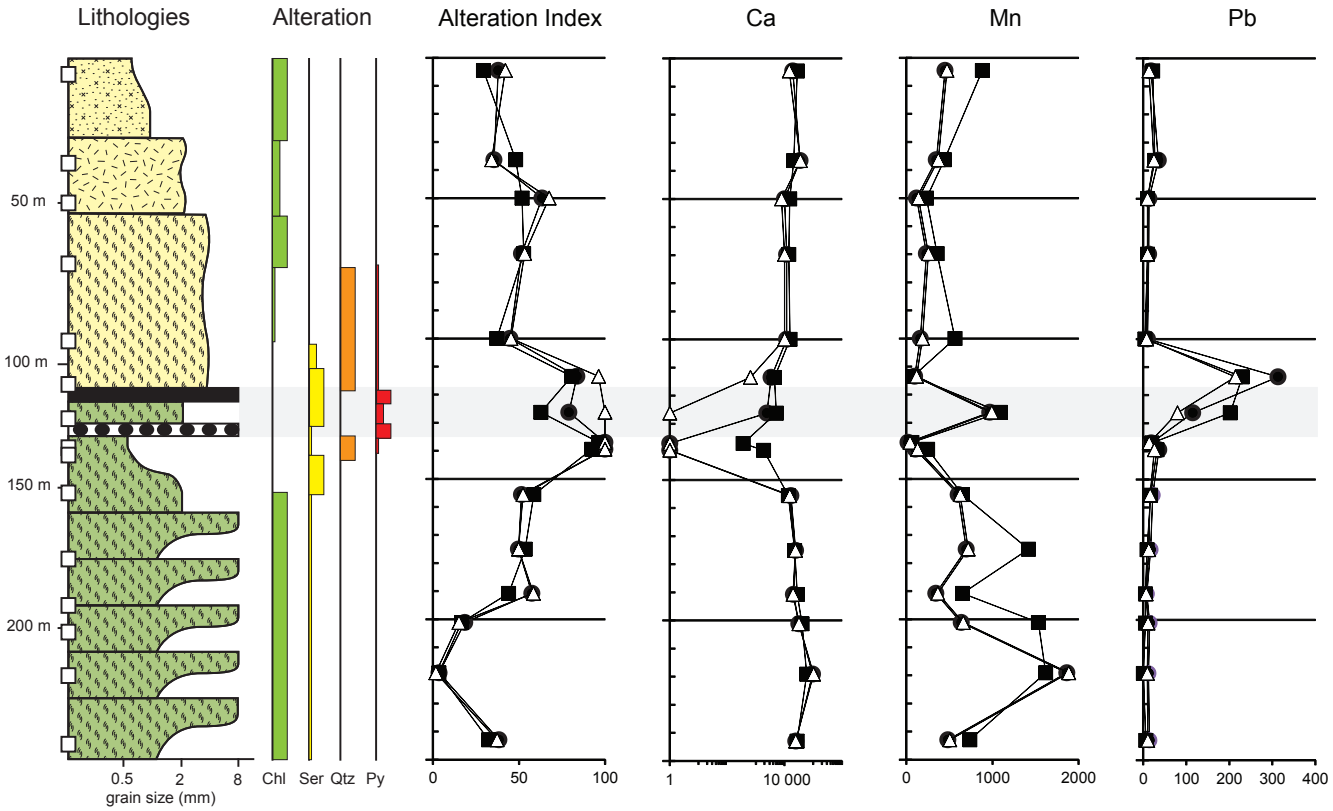

Figure 7. *Graphic log of TL11-05 with representative downhole plots using laboratory whole-rock data (black squares), uncorrected pXRF data (black circles), and corrected pXRF data (white triangles). Ca, Mn, and Pb in ppm. Lithology and alteration legend same as Figure 2, grey is mineralized and highly altered interval.*

AI values, they can be used to monitor the effects of hydrothermal alteration. Figure 8b plots the corrected pXRF analytical data using the modified formulas for thin section off-cuts. These values are similar to those derived from laboratory whole-rock data. Figure 8a and b both show a sericite hydrothermal alteration trend (1), followed by a sericite-chlorite-pyrite alteration trend (2) for the lower volcanic series, whereas the upper volcanic series shows either diagenetic trends (7 and 8) or a carbonate-sericite trend (5). This supports the observations in core that show increasing quartz + pyrite ± sericite underneath mineralization.

CONCLUSIONS

The main goals of this study were to evaluate the accuracy of the pXRF using diamond drill core samples and to evaluate the utility of pXRF generated data for VMS exploration. Portable XRF analyses generally have high determination coefficients ($R^2 \geq 0.7$) with laboratory whole-rock analyses for both pulps and thin section off-cuts and are reliably corrected by applying a linear correction.

Elements such as Cl, Nb, Ni, Pd, and Pt are below the lower limit of detection in all of the pXRF analyses; other elements are above the lower limit of detection but do not correlate well due to poor precision and accuracy as a result of either analyser issues (Ag and Au) or nugget effects (Cd, Mo, P, Sb, and Sn). This study found that pXRF data for off-cuts have slightly lower R^2 values for nearly every reliable element than pXRF data for pulps due to a subtle nugget effect in the off-cuts, but the difference in abundance is commonly ±35%. This study concludes that using diamond drill core (based on off-cuts as a proxy) is reasonable, but an effort must be made to avoid unrepresentative analysis sites (*e.g.*, clasts or phenocrysts). Of the elements available in 'soil mode' on the pXRF used, 13 of them are considered to be particularly suited to VMS exploration. Ti and Zr are reliable and are good discriminators of magmatic fractionation, allowing discrimination of felsic vs. mafic compositions. As, Ba, Ca, Co, Cu, Fe, K, Mn, Pb, Rb, S, and Sr are all reliable and, though not universally present in abundances above their lower limits of detection, their distributions generally vary with distance from mineralization, allowing the elements

to be used either individually or combined into ratios to monitor effects of hydrothermal alteration. The pXRF shows particular promise for use during VMS exploration field programs by allowing real-time acquisition of valuable geochemical data that could help direct concurrent exploration activities. However, results are not of high enough quality to allow the pXRF to replace traditional whole-rock analytical methods.

ACKNOWLEDGEMENTS

The authors wish to thank Arcus Development Group Inc. for allowing access to the property and core. Heather Burrell of Archer, Cathro and Associates (1981) Ltd. was a great help in getting us set up and telling us where the perfectly stacked core would be found. Mel and Will Fellers are thanked for their help with logistics, fine hospitality, and for renting us the 'ether hog' that got us around. Reviewers, Jan Peter and Jim Ryan of the Geological Survey of Canada, and Lee Pigage of the Yukon Geological Survey are thanked for critical reviews and discussion. Funding for the analytical portion of this study was provided by the Canadian Northern Economic Development Agency (CanNor) from the Strategic Investment in Northern Economic Development fund (SINED).

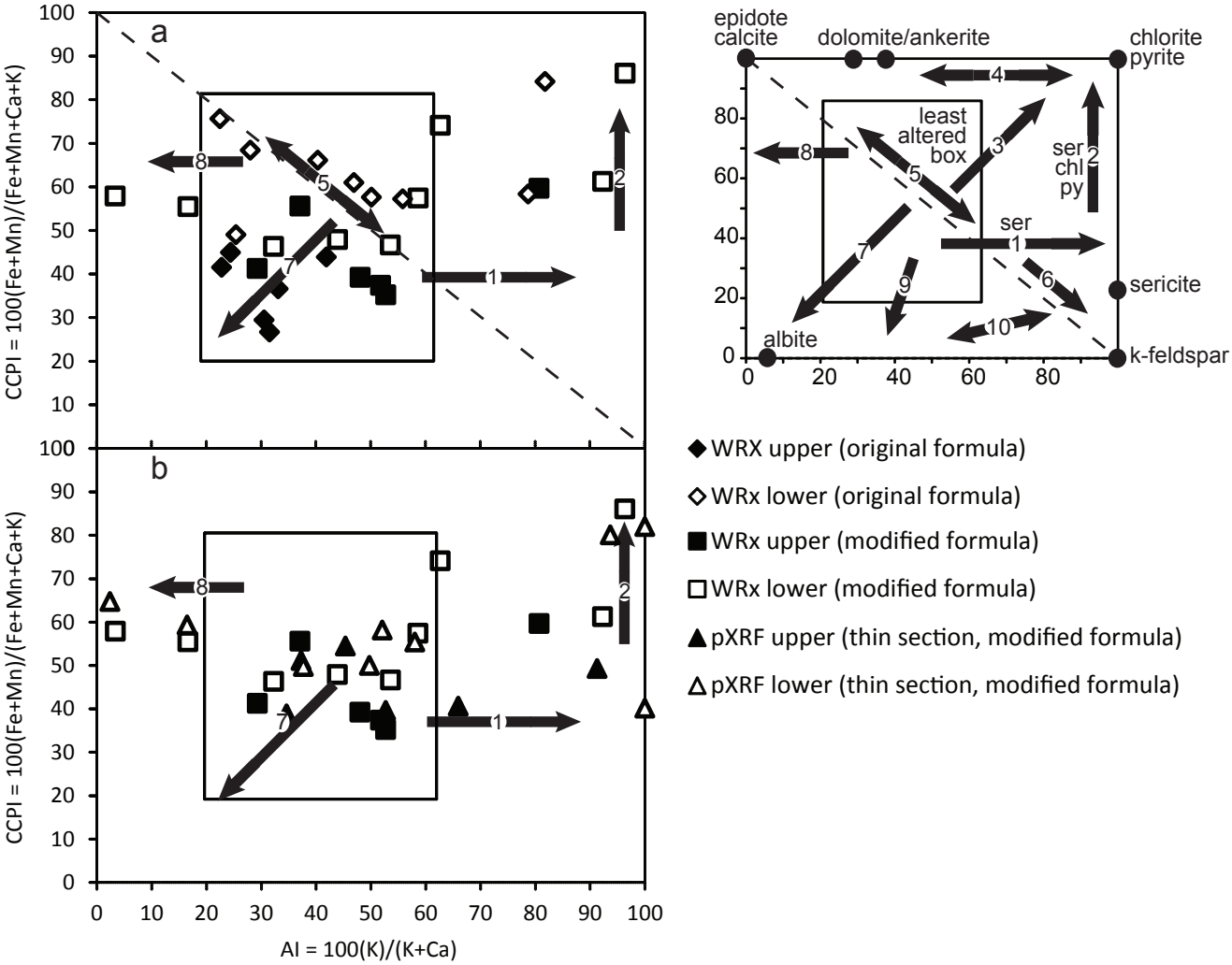

Figure 8. *Alteration box plot modified for pXRF elements. a) Points generated with formulas modified for pXRF data and the original formulas using whole-rock data; b) Points generated with pXRF modified formulas using corrected pXRF off-cut data and laboratory whole-rock data. Trends to the upper right of the dashed line are hydrothermal alteration trends (1 through 6) and trends to the lower left are diagenetic alteration trends (7 through 10), for further explanation of alteration trends see Large et al. (2001).*

REFERENCES

Barrett, T.J. and MacLean, W.H., 1999. Volcanic sequences, litho-geochemistry, and hydrothermal alteration in some bimodal volcanic-associated massive sulfide systems. *In:* Volcanic-associated massive sulfide deposits: processes and examples in modern and ancient settings, C.T. Barrie and M.D. Hannington (eds.), Society of Economic Geologists, vol. 8, p. 101-131.

Barrett, T.J., Cattalani, S., and Maclean, W.H., 1993. Volcanic lithogeochemistry and alteration at the Delbridge massive sulfide deposit, Noranda, Quebec. Journal of Geochemical Exploration, vol. 48, p. 135-173.

Chapman, J.B., Peter, J.M., Layton-Matthews, D., and Gemmell, J.B., 2009. Geochemistry of Archean sulfidic black shale horizons: combining data at multiple scales for improved targeting in VMS exploration. *In:* Proceedings of the 24th International Applied Geochemistry Symposium, D.R. Lentz, K.G. Thorne, and K.-L. Beal (eds.), Fredericton, New Brunswick, Canada, vol. 1, p. 19-22.

Gifkins, C., Herrmann, W., and Large, R., 2005. Altered volcanic rocks: A guide to description and interpretation, Centre for Ore Deposit Research (CODES), University of Tasmania, 275 p.

Gordey, S.P. and Ryan, J.J., 2005. Geology, Stewart River Area (115N, 115O and part of 115J), Yukon Territory. Geological Survey of Canada, scale 1:250 000.

Hunt, J.A., 2002. Volcanic-associated massive sulphide (VMS) mineralization in the Yukon-Tanana Terrane and coeval strata of the North American miogeocline, in the Yukon and adjacent areas. Exploration and Geological Services Division, Yukon Region, Indian and Northern Affairs Canada, 107 p.

Innov-X-Systems, 2009. Omega handheld XRF analyzer user manual, June 2009 edition.

Ishikawa, Y., Sawaguchi, T., Iwaya, S., and Horiuchi, M., 1976. Delineation of prospecting targets for Kuroko deposits based on modes of volcanism of underlying dacite and alteration haloes. Mining Geology, vol. 26, p. 105-117.

Large, R.R., Gemmell, J.B., Paulick, H., and Herrmann, W., 2001. The alteration box plot; a simple approach to understanding the relationship between alteration mineralogy and lithogeochemistry associated with volcanic-hosted massive sulfide deposits. Economic Geology and the Bulletin of the Society of Economic Geologists, vol. 96, p. 957-971.

MacLean, W.H. and Barrett, T.J., 1993. Lithogeochemical techniques using immobile elements. Journal of Geochemical Exploration, vol. 48, p. 109-133.

Mireku, L.K. and Stanley, C.R., 2006. Lithogeochemistry and hydrothermal alteration at the Halfmile Lake South Deep zone, a volcanic-hosted massive sulfide deposit, Bathurst mining camp, New Brunswick. Exploration and Mining Geology, vol. 15, p. 177-199.

Newberry, R.J., Brew, D.A., and Crafford, T.C., 1989. Zoned footwall alteration and original rock types at the Greens Creek volcanogenic massive sulfide (VMS) deposit, southeast Alaska. Proceedings to the Alaska Miners Association Juneau Conference, Juneau, Alaska, p. 29-31.

Pearce, J.A., 1996. A user's guide to basalt discrimination diagrams. *In:* Trace element geochemistry of volcanic rocks, D.A. Wyman (ed.), Volume Short Course Notes, Geological Association of Canada, Mineral Deposits Division, vol. 12, p. 79-113.

Peter, J.M., Mercier-Langevin, P., and Chapman, J.B., 2009. Application of field-portable x-ray fluorescence spectrometers in mineral exploration, with examples from the Abitibi Greenstone Belt. *In:* Proceedings of the 24th International Applied Geochemistry Symposium, D.R. Lentz, K.G. Thorne, and K.-L. Beal (eds.), Fredericton, New Brunswick, Canada, vol. 1, p. 83-86.

Ross, P.-S. and Bedard, J.H., 2009. Magmatic affinity of modern and ancient subalkaline volcanic rocks determined from trace-element discriminant diagrams. Canadian Journal of Earth Sciences, vol. 46, p. 823-839.

Ryan, J.J. and Gordey, S.P., 2001a. Geology, Thistle Creek area, Yukon Territory (115O/3). Geological Survey of Canada, scale 1:50 000.

Ryan, J.J. and Gordey, S.P., 2001b. New geological mapping in Yukon-Tanana terrane near Thistle Creek, Stewart River map area, Yukon Territory. Geological Survey of Canada, Current Research 2001-A2, 18 p.

Winchester, J.A. and Floyd, P.A., 1977. Geochemical discrimination of different magma series and their differentiation products using immobile elements. Chemical Geology, vol. 20, p. 325-343.

APPENDIX 1: Whole-rock analytical data.

	Detection Limit	Drillhole	TL11-05	TL11-05	TL11-05	TL11-05	TL11-05	TL11-05	TL11-05	TL11-05	TL11-05	TL11-05	TL11-05	TL11-05	TL11-05	TL11-05	TL11-05
		Depth (m)	4.50	36.36	50.00	69.76	99.97	113.50	126.25	137.00	139.45	155.60	175.07	190.75	201.20	219.10	243.00
		Sample No.	TL11-05-004.50m	TL11-05-036.36m	TL11-05-050.00m	TL11-05-069.76m	TL11-05-099.97m	TL11-05-113.50m	TL11-05-126.25m	TL11-05-137.00m	TL11-05-139.45m	TL11-05-155.60m	TL11-05-175.07m	TL11-05-190.75m	TL11-05-201.20m	TL11-05-219.10m	TL11-05-243.00m
SiO_2 (%)	0.01	FUS-ICP	71.48	69.76	73.39	71.72	74.55	56.81	74.48	78.73	70.17	69.38	66.56	66.95	62.36	54.62	71.1
Al_2O_3 (%)	0.01	FUS-ICP	13.44	13.75	14.24	14.25	12.41	24.77	12.83	4.96	12.1	12.57	14.23	14.36	13.73	15.23	13.46
Fe_2O_3* (%)	0.01	FUS-ICP	3.8	3.67	2.66	2.26	4.33	4.84	5.49	8.66	5.39	6.26	5.82	6.38	8.49	11.89	4.82
MnO (%)	0.001	FUS-ICP	0.114	0.057	0.03	0.046	0.073	0.01	0.141	0.008	0.032	0.084	0.183	0.084	0.198	0.209	0.095
MgO (%)	0.01	FUS-ICP	0.78	0.62	0.5	0.67	0.85	0.43	0.45	0.13	0.5	1.29	1.6	1.53	2.57	3.73	0.69
CaO (%)	0.01	FUS-ICP	3.87	2.94	2.13	1.97	2.17	0.62	0.72	0.05	0.26	1.91	3.13	3.87	5.71	8.34	3.78
Na_2O (%)	0.01	FUS-ICP	3.67	3.49	3.89	3.88	3.86	3.35	1.57	0.26	0.67	1.8	0.77	0.99	2.7	3.41	3.1
K_2O (%)	0.01	FUS-ICP	1.38	2.34	1.97	1.89	1.1	2.23	1.04	1.14	2.67	2.33	3.11	2.61	0.98	0.25	1.55
TiO_2 (%)	0.001	FUS-ICP	0.304	0.42	0.418	0.484	0.46	1.123	0.697	0.215	0.506	0.508	0.556	0.73	0.663	0.95	0.467
P_2O_5 (%)	0.01	FUS-ICP	0.07	0.11	0.1	0.08	0.09	0.03	0.07	0.02	0.15	0.09	0.13	0.13	0.13	0.16	0.11
LOI		FUS-ICP	1.96	2.33	1.55	1.74	0.73	5.25	3.25	5.2	5.41	3.89	2.58	1.92	1.52	0.88	1.32
Total			**100.9**	**99.49**	**100.9**	**98.98**	**100.6**	**99.45**	**100.7**	**99.37**	**97.85**	**100.1**	**98.67**	**99.56**	**99.06**	**99.67**	**100.5**
Sc (ppm)	1	FUS-ICP	9	11	8	14	11	23	13	6	14	15	25	20	25	36	14
Be (ppm)	1	FUS-ICP	2	2	2	< 1	1	2	< 1	< 1	< 1	1	< 1	< 1	< 1	< 1	1
V (ppm)	5	FUS-ICP	25	21	19	23	12	127	89	37	103	92	93	194	211	371	39
Sr (ppm)	2	FUS-ICP	153	111	98	94	86	310	140	26	71	82	63	120	129	499	104
Ba (ppm)	3	FUS-ICP	407	623	728	532	446	4175	2856	1873	4702	1112	887	1044	262	52	600
Cr (ppm)	20	FUS-MS	< 20	< 20	< 20	< 20	< 20	220	< 20	< 20	30	< 20	< 20	< 20	< 20	< 20	< 20
Co (ppm)	1	FUS-MS	3	1	1	1	2	12	4	10	6	6	9	11	20	31	6
Ga (ppm)	1	FUS-MS	17	19	19	17	15	28	19	10	13	14	15	18	17	20	16
Ge (ppm)	0.5	FUS-MS	1.7	1.5	1.6	1.3	1.7	2.6	6.1	1.1	0.6	0.8	1.3	1.6	1.8	2.2	1.5
As (ppm)	5	FUS-MS	< 5	< 5	< 5	< 5	< 5	8	19	< 5	10	< 5	< 5	< 5	< 5	< 5	< 5
Rb (ppm)	1	FUS-MS	31	59	41	45	20	40	24	20	61	49	56	54	26	2	37
Y (ppm)	0.5	FUS-MS	35.2	64.4	39.9	56.7	43.1	9.4	12.4	9.9	14.9	38.1	28.9	28.8	26.3	23.4	33.8
Zr (ppm)	1	FUS-MS	275	287	296	242	220	265	160	51	132	169	150	145	114	76	181
Nb (ppm)	0.2	FUS-MS	16.6	9.2	9.2	13.1	9.2	11.9	5.1	1.5	3.5	6.1	6.6	6.5	2.5	0.8	5.8
Mo (ppm)	2	FUS-MS	< 2	< 2	< 2	< 2	< 2	14	2	6	< 2	< 2	< 2	< 2	< 2	< 2	< 2
In (ppm)	0.1	FUS-MS	< 0.1	< 0.1	< 0.1	< 0.1	< 0.1	< 0.1	0.1	< 0.1	< 0.1	< 0.1	< 0.1	< 0.1	< 0.1	< 0.1	< 0.1
Sn (ppm)	1	FUS-MS	4	3	3	3	2	2	1	< 1	< 1	1	< 1	1	< 1	< 1	2
Sb (ppm)	0.2	FUS-MS	< 0.2	< 0.2	< 0.2	< 0.2	< 0.2	13.2	5.1	1.5	1	0.4	< 0.2	< 0.2	< 0.2	< 0.2	< 0.2
Cs (ppm)	0.1	FUS-MS	0.8	1.3	0.9	1.1	0.5	0.6	0.6	0.2	0.9	0.5	1.6	0.7	0.7	0.1	1.1
La (ppm)	0.05	FUS-MS	90.2	32.1	21.1	24.5	34.4	7.36	9.68	9.66	4.45	16.2	16.5	18.3	11.9	11.1	20.2
Ce (ppm)	0.05	FUS-MS	169	67.2	48	54	70.4	13.2	19.7	18.6	8.45	36.8	35.7	39.5	26.9	25.4	42.7
Pr (ppm)	0.01	FUS-MS	18.2	9.03	6.31	6.88	8.3	1.3	2.48	2.02	1.17	4.87	4.38	4.97	3.55	3.51	5.19
Nd (ppm)	0.05	FUS-MS	59.5	35.4	26.3	28.2	31.1	4.32	9.98	7.15	10.5	20.9	18	19.6	15.2	14.2	20.3
Sm (ppm)	0.01	FUS-MS	9.13	8.55	6.48	6.84	6.7	0.75	1.03	1.2	4.38	5.24	4.12	4.76	3.58	3.66	4.7
Eu (ppm)	0.01	FUS-MS	2.1	1.85	1.47	1.56	1.59	0.192	0.175	0.471	0.739	1.39	1.11	1.18	0.979	1.18	1.08
Gd (ppm)	0.01	FUS-MS	7.89	9.49	6.76	7.99	6.95	0.84	0.58	1.47	2.3	5.71	4.65	5.46	4.18	3.91	4.95
Tb (ppm)	0.01	FUS-MS	1.22	1.72	1.21	1.38	1.22	0.17	0.14	0.26	0.39	1	0.79	0.91	0.69	0.68	0.89
Dy (ppm)	0.01	FUS-MS	7.29	11	7.62	9.01	7.69	1.28	1.21	1.64	2.58	6.51	5.01	5.48	4.33	4.19	5.65
Ho (ppm)	0.01	FUS-MS	1.39	2.33	1.59	1.97	1.59	0.33	0.37	0.34	0.56	1.39	1.07	1.08	0.91	0.87	1.18
Er (ppm)	0.01	FUS-MS	3.97	7.05	4.82	6.2	4.67	1.23	1.52	1.02	1.76	4.23	3.29	3.02	2.77	2.61	3.58
Tm (ppm)	0.01	FUS-MS	0.567	1.09	0.723	0.955	0.701	0.243	0.316	0.154	0.286	0.637	0.508	0.422	0.425	0.389	0.546
Yb (ppm)	0.01	FUS-MS	3.76	7.17	4.88	6.53	4.68	2.02	2.71	1.02	2	4.27	3.39	2.66	2.84	2.61	3.7
Lu (ppm)	0.002	FUS-MS	0.592	1.17	0.784	1.03	0.743	0.357	0.486	0.162	0.343	0.682	0.552	0.4	0.451	0.426	0.609
Hf (ppm)	0.1	FUS-MS	8.1	7.7	7.5	6.7	6	7.7	4.2	1.4	3.6	4	3.9	3.8	3.1	2.2	5

APPENDIX 1 (continued): Whole-rock analytical data.

	Detection Limit	Drillhole	TL11-05	TL11-05	TL11-05	TL11-05	TL11-05	TL11-05	TL11-05	TL11-05	TL11-05	TL11-05	TL11-05	TL11-05	TL11-05	TL11-05	TL11-05
		Depth (m)	4.50	36.36	50.00	69.76	99.97	113.50	126.25	137.00	139.45	155.60	175.07	190.75	201.20	219.10	243.00
		Sample No.	TL11-05-004.50m	TL11-05-036.36m	TL11-05-050.00m	TL11-05-069.76m	TL11-05-099.97m	TL11-05-113.50m	TL11-05-126.25m	TL11-05-137.00m	TL11-05-139.45m	TL11-05-155.60m	TL11-05-175.07m	TL11-05-190.75m	TL11-05-201.20m	TL11-05-219.10m	TL11-05-243.00m
Ta (ppm)	0.01	FUS-MS	0.53	0.65	0.6	0.99	0.54	0.79	0.42	0.12	0.32	0.37	0.39	0.5	0.18	< 0.01	0.4
W (ppm)	0.5	FUS-MS	1.2	1.1	< 0.5	< 0.5	< 0.5	3.6	< 0.5	2	2.1	1	< 0.5	1.5	< 0.5	< 0.5	< 0.5
Tl (ppm)	0.05	FUS-MS	0.18	0.32	0.32	0.34	0.21	6.77	8.09	2.3	3.28	0.46	0.41	0.37	0.19	< 0.05	0.18
Bi (ppm)	0.1	FUS-MS	0.2	0.2	< 0.1	< 0.1	< 0.1	< 0.1	0.3	0.6	< 0.1	0.1	< 0.1	< 0.1	< 0.1	< 0.1	< 0.1
Th (ppm)	0.05	FUS-MS	11.8	7.42	6.81	6.12	6.03	1.44	3.05	1.58	0.59	5.01	4.11	4.16	2.47	1.17	4.93
U (ppm)	0.01	FUS-MS	0.99	1.88	1.87	1.65	1.32	3	0.75	0.94	3.72	1.85	1.24	1.16	0.76	0.36	1.35
Au (ppb)	2	INAA	4	< 2	< 2	< 2	< 2	< 2	8	412	62	< 2	< 2	< 2	< 2	< 2	< 2
As (ppm)	0.5	INAA	< 0.5	0.8	1.5	< 0.5	< 0.5	12.7	16.5	5.5	16	1.9	< 0.5	1.6	< 0.5	< 0.5	0.9
Br (ppm)	0.5	INAA	< 0.5	< 0.5	< 0.5	< 0.5	< 0.5	< 0.5	< 0.5	< 0.5	< 0.5	< 0.5	< 0.5	< 0.5	< 0.5	< 0.5	< 0.5
Cr (ppm)	5	INAA	< 5	< 5	< 5	< 5	6	252	15	< 5	34	< 5	18	< 5	6	< 5	< 5
Ir (ppb)	5	INAA	< 5	< 5	< 5	< 5	< 5	< 5	< 5	< 5	< 5	< 5	< 5	< 5	< 5	< 5	< 5
Sc (ppm)	0.1	INAA	8.3	10.8	7.4	13.2	10.5	23	11.3	6.4	14.2	15.3	23.8	19.5	26.2	34.9	13.5
Se (ppm)	3	INAA	< 3	< 3	< 3	< 3	< 3	< 3	< 3	9	< 3	< 3	< 3	< 3	< 3	< 3	< 3
Sb (ppm)	0.2	INAA	< 0.2	0.3	< 0.2	< 0.2	< 0.2	19.5	4.6	2	2	0.3	< 0.2	< 0.2	< 0.2	< 0.2	< 0.2
Ni (ppm)	1	TD-ICP	3	3	3	4	3	39	6	12	11	2	14	7	11	12	2
Cu (ppm)	1	TD-ICP	6	16	17	2	12	44	224	7430	299	9	31	11	71	136	5
Zn (ppm)	1	TD-ICP	90	69	56	33	93	62	245	104	209	44	192	103	101	89	73
Cd (ppm)	0.5	TD-ICP	< 0.5	< 0.5	< 0.5	< 0.5	< 0.5	< 0.5	0.7	0.9	0.8	< 0.5	0.7	< 0.5	< 0.5	0.6	< 0.5
S (%)	0.001	TD-ICP	0.024	0.016	0.182	0.015	0.106	2.71	0.427	7.37	3.97	3.38	0.61	0.036	0.069	0.062	0.027
Ag (ppm)	0.3	TD-ICP	< 0.3	< 0.3	< 0.3	< 0.3	< 0.3	< 0.3	< 0.3	1.7	< 0.3	< 0.3	< 0.3	< 0.3	< 0.3	< 0.3	< 0.3
Pb (ppm)	3	TD-ICP	22	27	10	10	4	230	202	20	32	17	9	5	5	< 3	6

**Total iron reported as Fe_2O_3*

Analytical methods described in Section 5.1

FUS-MS = lithium metaborate/tetraborate Fusion - Inductively Coupled Plasma Mass Spectrometry

FUS-ICP = lithium metaborate/tetraborate Fusion - Inductively Coupled Plasma Optical Emission Spectrometry

TD-ICP = Total Digestion - Inductively Coupled Plasma Optical Emission Spectrometry

INAA = Instrumental Neutron Activation Analysis of pulp (no digestion/fusion)

Samples were crushed, split and then pulverized in a mild steel mill

Analysis below lower detection limits shown with a "<" detection limit value

Details of diamond drill hole TL11-05:

UTM collar coordinates: 594353 E, 6987715 N, Zone 7, Datum NAD83

Azimuth: 360°

Dip: -45°

APPENDIX 2: Portable x-ray fluorescence spectrometer (pXRF) pulp and off-cut data.

Drillhole	TL11-05		TL11-05		TL11-05		TL11-05		TL11-05		TL11-05		TL11-05		TL11-05	
Depth (m)	4.50		36.36		50.00		69.76		99.97		113.50		126.25		137.00	
Sample No.	TL11-05-004.50m		TL11-05-036.36m		TL11-05-050.00m		TL11-05-069.76m		TL11-05-099.97m		TL11-05-113.50m		TL11-05-126.25m		TL11-05-137.00m	
	raw	corr.	raw	corr.	raw	corr.	raw	corr.	raw	corr.	raw	corr.	raw	corr.	raw	corr.
Ag-pulp	128	NA	117	NA	118	NA	104	NA	133	NA	147	NA	235	NA	240	NA
Ag-TS	148	NA	202	NA	129	NA	114	NA	118	NA	210	NA	127	NA	154	NA
As-pulp	2	BD	2	BD	1	BD	2	BD	2	BD	11	1.8	60	16.8	4	BD
As-TS	2.5	BD	1.8	BD	0.4	BD	2.5	BD	2.5	BD	17.2	3.6	8.4	0.9	1.7	BD
Au-pulp	BD	BD	BD	BD	BD	BD	BD	BD	BD	BD	BD	BD	BD	BD	BD	BD
Au-TS	BD	BD	BD	BD	BD	BD	BD	BD	BD	BD	BD	BD	BD	BD	BD	BD
Ba-pulp	319	334	285	285	332	353	240	220	237	216	1753	2413	2701	3788	828	1072
Ba-TS	298	304	383	428	375	416	226	200	220	192	2203	3066	1277	1724	786	1012
Ca-pulp	19025	17950	15285	13798	10613	8613	9538	7419	11072	9122	2749	BD	3060	228	25	BD
Ca-TS	19339	18298	34978	35657	9919	7843	11809	9940	11845	9980	3437	647	2439	BD	25	BD
Cd-pulp	24	BD	5	BD	22	BD	17	BD	28	0.03	11	BD	63	0.38	52	0.27
Cd-TS	9	BD	30	0.05	22	BD	21	BD	16	BD	18	BD	6	BD	4	BD
Co-pulp	316	9	287	9	167	6	151	6	346	10	420	11	860	20	1077	24
Co-TS	251	8	321	9	138	6	107	5	193	7	248	8	214	7	546	14
Cr-pulp	54	111	31	81	28	77	31	82	34	85	207	314	55	113	33	84
Cr-TS	19	65	12	57	37	89	18	64	15	60	192	294	53	111	39	92
Cu-pulp	BD	BD	BD	BD	BD	BD	BD	BD	BD	BD	BD	BD	400	381	7895	7427
Cu-TS	BD	BD	BD	BD	BD	BD	BD	BD	BD	BD	BD	BD	55	57	7184	6758
Fe-pulp	20228	29394	20516	30001	14256	16793	13013	14171	23707	36735	20427	29814	29166	48253	50956	94231
Fe-TS	16871	22311	18509	25768	10336	8522	9060	5830	13238	14646	10781	9460	18904	26601	20386	29727
K-pulp	8523	7103	14732	13685	12074	10867	10753	9467	6379	4831	14447	13383	6882	5364	7726	6258
K-TS	11795	10572	19199	18420	17144	16241	12499	11318	9610	8256	17543	16664	9155	7773	9167	7786
Mn-pulp	739	762	387	409	226	249	323	345	490	512	129	151	811	833	79	101
Mn-TS	450	473	349	371	118	141	234	256	163	185	95	118	969	991	20	42
Mo-pulp	BD	NA	BD	NA	BD	NA	BD	NA	BD	NA	18	NA	8	NA	14	NA
Mo-TS	BD	NA	BD	NA	BD	NA	BD	NA	BD	NA	22	NA	BD	NA	24	NA
Nb-pulp	BD	NA	BD	NA	BD	NA	BD	NA	BD	NA	BD	NA	BD	NA	BD	NA
Nb-TS	BD	NA	BD	NA	BD	NA	BD	NA	BD	NA	BD	NA	BD	NA	BD	NA
Ni-pulp	BD	NA	BD	NA	BD	NA	BD	NA	BD	NA	BD	NA	BD	NA	BD	NA
P-pulp	BD	NA	BD	NA	BD	NA	BD	NA	BD	NA	BD	NA	BD	NA	BD	NA
P-TS	BD	NA	BD	NA	BD	NA	BD	NA	BD	NA	BD	NA	BD	NA	BD	NA
Pb-pulp	26	18	30	21	15	11	18	13	13	9	257	175	356	243	26	18
Pb-TS	18	13	35	25	13	10	13	10	10	8	313	214	115	79	19	14
Rb-pulp	32	13	61	32	42	20	47	23	21	6	42	20	48	24	22	6
Rb-TS	35	15	72	40	43	20	36	16	18	4	56	29	23	7	21	6
S-pulp	BD	BD	BD	BD	BD	BD	BD	BD	BD	BD	8287	17528	1985	2341	32340	75495
S-TS	BD	BD	BD	BD	BD	BD	BD	BD	BD	BD	25080	57999	1173	382	64612	153270
Sb-pulp	BD	NA	BD	NA	BD	NA	BD	NA	BD	NA	7	NA	BD	NA	BD	NA
Sn-pulp	16	NA	21	NA	19	NA	25	NA	27	NA	47	NA	48	NA	41	NA
Sn-TS	28	NA	27	NA	4	NA	21	NA	17	NA	31	NA	9	NA	BD	NA
Sr-pulp	146	155	105	113	94	102	93	101	83	91	305	315	260	269	27	35
Sr-TS	96	104	167	176	89	97	76	84	73	80	377	387	83	91	22	29
Ta-pulp	33	NA	33	NA	39	NA	33	NA	30	NA	54	NA	33	NA	5	NA
Ta-TS	29	NA	40	NA	36	NA	28	NA	24	NA	63	NA	18	NA	2	NA
Ti-pulp	1422	1506	2006	2155	1832	1961	2198	2368	2102	2261	5508	6041	3985	4351	1727	1845
Ti-TS	1528	1623	1870	2003	2082	2239	2359	2546	2005	2153	5703	6258	3255	3541	1809	1935
V-pulp	59	NA	56	NA	58	NA	50	NA	45	NA	306	NA	224	NA	146	NA
V-TS	34	NA	45	NA	70	NA	42	NA	41	NA	296	NA	244	NA	121	NA
Y-pulp	77	13	357	61	163	28	365	62	171	29	BD	BD	BD	BD	BD	BD
Y-TS	9	2	337	57	137	23	154	26	53	9	BD	BD	BD	BD	BD	BD
Zn-pulp	75	BD	56	BD	43	BD	27	BD	77	BD	56	BD	545	174	92	BD
Zn-TS	56	BD	52	BD	22	BD	22	BD	50	BD	73	BD	69	BD	108	BD
Zr-pulp	315	260	324	267	319	263	275	226	242	199	301	248	362	298	60	48
Zr-TS	318	262	572	472	375	309	231	190	243	199	396	327	107	86	62	50

Analytical methods described in Section 5.2

BD = below lower limit of detection

corr. = corrected data using slope and y-intercept values in Table 2

NA in corrected column indicates data had R^2 value too low (<0.5) to apply linear correction

All data in ppm and elemental form

APPENDIX 2 (continued): Portable x-ray fluorescence spectrometer (pXRF) pulp and off-cut data.

Drillhole	TL11-05		TL11-05		TL11-05		TL11-05		TL11-05		TL11-05		TL11-05	
Depth (m)	139.45		155.60		175.07		190.75		201.20		219.10		243.00	
Sample No.	TL11-05-139.45m		TL11-05-155.60m		TL11-05-175.07m		TL11-05-190.75m		TL11-05-201.20m		TL11-05-219.10m		TL11-05-243.00m	
	raw	corr.	raw	corr.	raw	corr.	raw	corr.	raw	corr.	raw	corr.	raw	corr.
Ag-pulp	204	NA	167	NA	160	NA	178	NA	185	NA	227	NA	127	NA
Ag-TS	138	NA	138	NA	161	NA	153	NA	158	NA	283	NA	140	NA
As-pulp	18	4.0	BD	BD	BD	BD	BD	BD	3	BD	BD	BD	1	BD
As-TS	6.0	0.2	2.5	BD	2.5	BD	0.8	BD	0.2	BD	2.2	BD	2.5	BD
Au-pulp	BD	BD	BD	BD	BD	BD	BD	BD	BD	BD	BD	BD	BD	BD
Au-TS	BD	BD	BD	BD	BD	BD	BD	BD	BD	BD	BD	BD	BD	BD
Ba-pulp	2939	4133	591	728	489	581	583	717	389	436	691	873	276	272
Ba-TS	3238	4567	575	705	450	525	716	910	323	340	884	1154	371	410
Ca-pulp	1266	BD	10209	8164	16133	14740	19714	18714	34127	34713	58013	61226	19505	18483
Ca-TS	25	BD	16587	15243	24476	24000	20616	19716	31526	31826	95467	102800	24781	24339
Cd-pulp	13	BD	19	BD	23	BD	16	BD	15	BD	4	BD	6	BD
Cd-TS	0	BD	7	BD	1	BD	0	BD	7	BD	21	BD	14	BD
Co-pulp	718	17	542	14	529	13	605	15	775	18	1305	29	394	11
Co-TS	225	7	397	11	333	10	400	11	411	11	1332	30	331	10
Cr-pulp	75	139	36	87	39	91	28	77	23	71	7	49	35	87
Cr-TS	48	104	26	74	18	64	27	76	14	58	-8	30	16	62
Cu-pulp	400	381	BD	BD	BD	BD	BD	BD	50	52	128	126	BD	BD
Cu-TS	144	141	BD	BD	BD	BD	BD	BD	BD	BD	322	308	BD	BD
Fe-pulp	21713	32528	29535	49033	32943	56223	37980	66850	50238	92715	73121	140998	26060	41700
Fe-TS	9558	6881	23767	36861	24898	39247	30460	50983	28475	46796	91830	180475	20613	30207
K-pulp	20403	19696	16990	16079	22932	22377	19364	18594	7578	6102	1490	BD	11215	9957
K-TS	23573	23057	17574	16697	24177	23696	27844	27583	7128	5625	3486	1764	15414	14408
Mn-pulp	280	302	581	604	1124	1146	527	550	1341	1364	1418	1440	642	664
Mn-TS	106	128	603	626	694	717	342	364	637	660	1865	1887	483	505
Mo-pulp	12	NA	BD	NA	BD	NA	BD	NA	BD	NA	4	NA	BD	NA
Mo-TS	6	NA	BD	NA	BD	NA	BD	NA	BD	NA	3	NA	BD	NA
Nb-pulp	BD	NA	BD	NA	BD	NA	BD	NA	BD	NA	BD	NA	BD	NA
Nb-TS	BD	NA	BD	NA	BD	NA	BD	NA	BD	NA	BD	NA	BD	NA
Ni-pulp	BD	NA	BD	NA	BD	NA	BD	NA	BD	NA	BD	NA	BD	NA
P-pulp	BD	NA	BD	NA	BD	NA	BD	NA	BD	NA	BD	NA	BD	NA
P-TS	BD	NA	BD	NA	BD	NA	BD	NA	BD	NA	BD	NA	BD	NA
Pb-pulp	60	42	23	16	17	13	11	9	13	9	17	12	14	10
Pb-TS	36	25	22	16	17	12	8	6	15	11	12	9	14	11
Rb-pulp	94	55	53	27	61	32	56	29	26	9	1	-8	37	16
Rb-TS	66	35	46	22	52	27	64	34	19	4	6	-4	41	19
S-pulp	11220	24597	10151	22019	2095	2604	BD	BD	BD	BD	BD	BD	BD	BD
S-TS	23241	53567	34437	80549	BD	BD	BD	BD	BD	BD	BD	BD	BD	BD
Sb-pulp	BD	NA	BD	NA	BD	NA	BD	NA	BD	NA	20	NA	4	NA
Sn-pulp	11	NA	10	NA	11	NA	14	NA	16	NA	19	NA	10	NA
Sn-TS	BD	NA	BD	NA	BD	NA	8	NA	BD	NA	8	NA	BD	NA
Sr-pulp	101	109	81	89	62	70	115	123	128	136	481	493	97	105
Sr-TS	59	67	82	90	64	72	93	101	111	119	502	514	98	106
Ta-pulp	30	NA	18	NA	37	NA	34	NA	29	NA	37	NA	29	NA
Ta-TS	25	NA	33	NA	28	NA	30	NA	24	NA	35	NA	28	NA
Ti-pulp	3860	4212	2831	3070	2937	3188	3903	4260	3409	3712	4475	4895	2437	2633
Ti-TS	4925	5395	3180	3457	2005	2154	3391	3692	2994	3251	4713	5159	2544	2752
V-pulp	343	NA	105	NA	95	NA	127	NA	85	NA	118	NA	53	NA
V-TS	523	NA	108	NA	74	NA	138	NA	67	NA	140	NA	64	NA
Y-pulp	BD	BD	152	26	38	6	BD	BD	BD	BD	BD	BD	95	16
Y-TS	BD	BD	148	25	31	5	BD	BD	BD	BD	BD	BD	BD	BD
Zn-pulp	228	40	38	BD	173	17	89	BD	92	BD	96	BD	61	BD
Zn-TS	48	BD	40	BD	169	16	52	BD	43	BD	121	BD	48	BD
Zr-pulp	180	147	186	152	168	137	166	136	127	103	85	68	210	172
Zr-TS	107	86	205	168	167	136	149	121	153	125	73	59	208	171